Green Chemistry

PAPER

View Article Online
View Journal | View Issue

Check for updates

Cite this: *Green Chem.*, 2021, **23**, 430

Molecular H_2O promoted catalytic bicarbonate reduction with methanol into formate over $Pd_{0.5}Cu_{0.5}$/C under mild hydrothermal conditions†

Xiaoguang Wang,[a] Yang Yang,[a] Heng Zhong, *[a,b,c] Tianfu Wang, [a,c] Jiong Cheng[a] and Fangming Jin *[a,b,c]

Received 14th August 2020,
Accepted 19th November 2020

DOI: 10.1039/d0gc02785e

rsc.li/greenchem

Direct reduction of bicarbonate, a typical product of CO_2 captured in alkaline solution, into value-added organics is one promising way to achieve a simplified and green CO_2 capture and utilization process. In this work, a new strategy of bicarbonate reduction coupled with methanol oxidation into a dual formation of formate under mild hydrothermal conditions is reported. A 68% formate production efficiency based on the reductant methanol and nearly 100% selectivity of formate were obtained *via* a $Pd_{0.5}Cu_{0.5}$/C catalyst at 180 °C. An *operando* hydrothermal ATR-FTIR study proved that the bicarbonate was reduced by the *in situ* generated hydrogen from methanol, which was stepwise oxidized to formaldehyde and formic acid. Notably, DFT calculations and a qNMR study of the ^{13}C and ^{2}H (D) isotopic labelling revealed that H_2O molecules not only supplied the hydrogen for bicarbonate reduction but also acted as an indispensable promoter to enhance the catalytic performance of $Pd_{0.5}Cu_{0.5}$/C for methanol activation.

Published on 19 novembro 2020. Downloaded on 03/09/2024 17:48:12.

1. Introduction

Reduction of CO_2, a typical greenhouse gas, to useful chemicals has shown considerable environmental and economic benefits since the fixation of CO_2 would significantly alleviate the associated environmental risks and the stress of fossil fuel depletion. Although the direct conversion of CO_2 from industrial flue gas has been reported,[1] CO_2 generally needs to be captured from either the atmosphere or point sources usually by using alkaline absorbents before further utilization. This process transforms CO_2 into HCO_3^- and/or CO_3^{2-} (the final products are pH dependent).[2,3] However, as shown in Fig. 1, the current technologies for CO_2 conversion are mainly limited to gaseous CO_2 transformation.[4–6] Thus, the captured CO_2 (in the form of HCO_3^- and/or CO_3^{2-}) needs to be regenerated and released at a relatively high dissociation temperature of *ca.* 200–1000 °C and re-compressed to high-pressure CO_2 gas before being subjected to these methods, which is not only complicated but also consumes a large amount of energy.[7] On the other hand, HCO_3^- is the dominant substance (nearly 100%) among all the dissolved carbon species (CO_2(aq), H_2CO_3, HCO_3^- and CO_3^{2-}) in a CO_2-saturated alkaline solution.[8] If the captured CO_2 could be converted directly into the form of HCO_3^-, not only would much energy be saved but also the process of CO_2 capture and utilization would be greatly simplified. Therefore, the direct reduction of HCO_3^- could be considered as a promising green strategy for CO_2 capture and utilization.

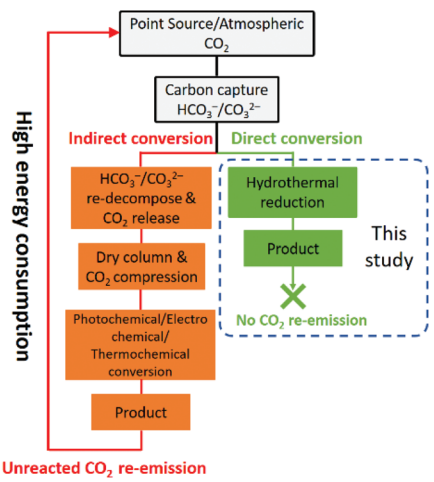

Fig. 1 Scheme of CO_2 capture and utilization – a comparison of previous methods and this study.

[a]*School of Environmental Science and Engineering, State Key Lab of Metal Matrix Composites, Shanghai Jiao Tong University, Shanghai 200240, China. E-mail: fmjin@sjtu.edu.cn, zhong.h@sjtu.edu.cn*
[b]*Center of Hydrogen Science, Shanghai Jiao Tong University, Shanghai, 200240, China*
[c]*Shanghai Institute of Pollution Control and Ecological Security, Shanghai 200092, P.R. China*

†Electronic supplementary information (ESI) available. See DOI: 10.1039/d0gc02785e

This journal is © The Royal Society of Chemistry 2021

Published on 19 novembro 2020. Downloaded on 03/09/2024 17:48:12.

Among the organics derived from CO_2/HCO_3^-, formic acid is one of the most important products due to its versatile application in modern chemical industry. More importantly, formic acid with a 4.4 wt% hydrogen content has been recently regarded as a promising hydrogen carrier because of its stability, low toxicity, biodegradability, and convenience in storage and transportation.[9,10] Current methods of formic acid production generally require fossil-based CO and extensive alkali, thus suffering from environmental risk and heavy reliance on fossil feedstock. Therefore, replacing CO with HCO_3^- in formic acid production, especially when driven by renewable energy, could be an ideal green and clean strategy.

For the CO_2/HCO_3^- reduction, high-pressure H_2 gas is usually an indispensable element, which is currently mainly derived from non-renewable natural gas and petroleum,[11,12] resulting in high energy consumption and environmental problems. In addition, the use of high-pressure H_2 gas involves energy consumption, storage, and transportation issues. On the other hand, biomass or their derivatives rich in reducing functional groups show great potential as renewable alternatives for molecular H_2, by acting as active hydrogen donors through the pathway known as aqueous re-forming with the assistance of hydrothermal reactions.[13,14] Meanwhile, a hydrothermal environment has been verified to show robustness for HCO_3^- reduction according to our previous works.[15,16] Thus, with the *in situ* generated hydrogen from biomass hydrothermal re-forming, HCO_3^- reduction is expected to be achieved in a H_2-free pathway under hydrothermal conditions.[17,18]

Methanol (CH_3OH) has wide application in chemical reactions, and can be easily produced from renewable sources such as biomass.[19] It has been reported that over 300 000 metric tons of methanol is annually produced from renewable resources in the United States.[20] Given that the functional group of –OH is stored in methanol, it can serve as a clean, efficient and renewable hydrogen source, which makes it a high-potential hydrogen source for HCO_3^- reduction. More importantly, as shown in eqn (1), HCO_3^- reduction with methanol can achieve a dual formation of formic acid/formate simultaneously, indicating that good energy efficiency and high atomic economy can be obtained.

$$CH_3OH + 2HCO_3^- \rightarrow HCOOH + 2HCOO^- + H_2O \quad (1)$$

$\Delta_rH^\ominus$ (298 K) = −74.7 kJ mol^{-1}; $\Delta_rG^\ominus$ (298 K) = −32.1 kJ mol^{-1}

$\Delta_rH^\ominus$ (453 K) = −49.7 kJ mol^{-1}; $\Delta_rG^\ominus$ (453 K) = −15.8 kJ mol^{-1}

While the overall reduction of HCO_3^- with methanol into formate is thermodynamically favourable, a reasonable catalyst is expected to drive the reaction more efficiently. Pd-based materials are well-known hydrogenation catalysts due to their excellent hydrogen absorption capacity;[21,22] however, the high cost and limited reserves have impeded their wide application. Diluting Pd with Earth-abundant materials is a feasible and facile strategy to decrease the cost of Pd-based catalysts and to further increase its catalytic performance and stability.[23,24] Cu is one of the most extensively studied metal catalysts for CO_2 hydrogenation.[25] Also, Cu has been reported to be efficient in activating alcohols due to the enrichment of the atomic oxygen species at the copper surface and sub-/near-surface regions to form a copper suboxide phase during the reaction, which can effectively bind and activate the alcohol molecules.[26,27] Therefore, combining the metallic Pd catalyst with Cu would probably be a logical strategy to catalyse the HCO_3^- reduction with methanol effectively.

In general, heterogeneous catalysts are the primary target for development due to their prominent role in catalysing the reaction. However, since the catalysis occurs at the interfacial sites, substances in liquid or gaseous phases can also affect the catalytic properties.[28] In a typical hydrothermal reaction, water is generally considered to be an environmentally benign medium due to its unique inherent properties of high ionic product (K_w) and low dielectric constant at high temperature and under high pressure.[29] However, beyond the well-known function as a solvent, there is evidence that water is indispensable for the hydrothermal conversion of biomass and HCO_3^- based on previous works,[30,31] but the mechanism is still unknown.

Here, we propose a new route to HCO_3^- reduction into formate with methanol as the reductant under mild hydrothermal conditions. Methanol was oxidized into formate simultaneously, which led to a dual formation of formate. The results showed that HCO_3^- could be reduced efficiently at 180 °C on a $Pd_{0.5}Cu_{0.5}/C$ catalyst. More importantly, H_2O was found to not only serve as an environmentally benign solvent, but also act as a bridge for methanol activation and oxidation to produce H_2 and thereby achieve HCO_3^- reduction. Also, immense efforts have been made in this research in exploring the role of H_2O with the aid of ^{13}C- and ^2H-qNMR and DFT studies. The present study proposes a new and green method of direct reduction of bicarbonate with alcohols as renewable hydrogen sources to achieve the dual formation of formic acid/formate in one step. These results could provide new insights into developing a simplified and greener process for CO_2 capture and utilization.

2. Experimental

2.1 Materials

Methanol (CH_3OH, 99.9%), palladium chloride ($PdCl_2$, 99.99%) and copper nitrate trihydrate ($Cu(NO_3)_2{\cdot}3H_2O$, 99.99%) were purchased from Shanghai Macklin Biochemical Technology Co., Ltd. Sodium bicarbonate ($NaHCO_3$, 99.9%) was purchased from Sinopharm Chemical Reagent Co., Ltd and was selected as the CO_2 source, considering that $NaHCO_3$ is the main product from trapping of CO_2 in waste streams by alkaline solutions. Cabot Vulcan XC-72 carbon was used as the catalyst support. D_2O (99.9%, Sinopharm Chemical Reagent Co.), $NaH^{13}\underline{C}O_3$ (99%, Sigma-Aldrich), $H^{13}\underline{C}OOH$ (≥95%, J Cambridge Isotope Laboratories Ltd) and $CH_3{}^{13}\underline{C}OOH$ (≥95%, J Cambridge Isotope Laboratories Ltd) were used for the deter-

Published on 19 novembro 2020. Downloaded on 03/09/2024 17:48:12.

mination of the formate source. All reagents were used without further purification. Deionized water was used throughout the study.

2.2 Catalyst preparation

$Pd_{0.5}Cu_{0.5}$/C catalyst with a 7.5 wt% total loading was prepared by an impregnation method. First, a certain amount of $PdCl_2$ was dissolved in 1 mol L^{-1} HCl to obtain a 0.2 mol L^{-1} H_2PdCl_4 solution. Then, 1.05 mL of 0.2 mol L^{-1} H_2PdCl_4 and 5 mL of 11.4 g L^{-1} $Cu(NO_3)_2{\cdot}3H_2O$ solution were slowly added into a 100 mL flask and mixed with 0.4625 g of carbon powder under vigorous stirring. The pH of the mixture was increased to 10 by adding 0.5 mol L^{-1} NaOH solution. After stirring for 24 h, 10 mL of 2 mol L^{-1} $NaBH_4$ was added dropwise into the mixture. After continuously stirring for another 12 h, the black suspension was filtered, washed with deionized water thoroughly and dried in a vacuum dryer to obtain the final $Pd_{0.5}Cu_{0.5}$/C catalyst. By keeping the total loading of metals (Pd and Cu) at 7.5 wt%, Pd–Cu catalysts with different molar ratios ($Pd_{0.75}Cu_{0.25}$/C, $Pd_{0.66}Cu_{0.33}$/C, $Pd_{0.33}Cu_{0.66}$/C and $Pd_{0.25}Cu_{0.75}$/C) were obtained; Pd/C and Cu/C were also prepared by using a similar method. The ICP-OES results of each catalyst are summarized in Table S1.†

2.3 Experimental procedures

In this study, all experiments were conducted in a stainless steel (SUS 316) tubular reactor (3/8 inch o.d., 1 mm wall thickness) with an inner volume of 5.7 mL. The schematic drawing of the reactor system can be found in our previous research.[32] A typical reaction procedure was as follows: 0.1 mol L^{-1} methanol, 1 mol L^{-1} $NaHCO_3$ and 50 mg catalyst were loaded into the reactor. Then, the reactor was sealed and placed in a salt bath, which was preheated to a desired temperature. After a certain reaction time, the reactor was removed out of the salt bath and quickly submerged in a cold-water bath to quench the reaction. The liquid and solid samples were separated through a 0.22 μm syringe filter and collected for further analysis. The gas sample was collected by a water–gas replacement method in a measuring cylinder immersed in a saturated NaCl aqueous solution tank.

In this study, the amount of formate obtained from HCO_3^- by one hydroxyl is used to evaluate the efficiency of $NaHCO_3$ reduction with methanol (abbreviated as 'formate production efficiency'). The detailed definition can be found in the ESI.†

2.4 Analytical methods

Liquid samples were analysed by high-performance liquid chromatography (HPLC), gas chromatography-mass spectrometry (GC-MS), gas chromatography-flame ionization detection (GC-FID) and $^{13}C/^{2}H$-quantitative nuclear magnetic resonance ($^{13}C/^{2}H$-qNMR). Gas samples were characterized by GC-MS and quantified using a gas chromatography-thermal conductivity detector (GC-TCD). Solid samples were analysed using an X-ray diffractometer (XRD), an X-ray photoelectron spectrometer (XPS) and a transmission electron microscope (TEM). *Operando* hydrothermal ATR-FTIR was used to monitor the reaction process (Fig. S1†). The detailed analytical conditions can be found in the ESI.†

3. Results and discussion

3.1 Characterization of catalysts

First, the $Pd_{0.5}Cu_{0.5}$/C catalyst was prepared and characterized. For comparison, a Pd/C catalyst was also synthesized by a similar procedure without adding the Cu precursor. The SEM image showed that nanoparticles (NPs) of *ca.* 100 nm were observed for the $Pd_{0.5}Cu_{0.5}$/C catalyst, which should be associated with the carbon support since similar morphologies were also observed for the Pd/C and carbon black particle samples (Fig. S2 and 3†). The TEM image of the $Pd_{0.5}Cu_{0.5}$/C catalyst showed that metal nanoparticles with an average diameter of 3.4 ± 0.3 nm were successfully dispersed on the carbon support (Fig. 2a). The composition of the NPs was verified by energy-dispersive X-ray spectroscopy (EDS) analysis, which clearly demonstrates that Cu and Pd atoms are randomly and homogeneously distributed in each NP (Fig. 2b–e), suggesting that the PdCu alloy was successfully formed. In a high-resolution TEM (HRTEM) image of a typical NP from $Pd_{0.5}Cu_{0.5}$/C (Fig. 2f), the measured lattice distance was 2.28 Å, which can be attributed to the 1/3(422) fringes of the PdCu alloy's face-centred cubic structure.[33–35] In addition, the Pd nanoparticles had an average diameter of 2.6 nm as seen from the TEM image of Pd/C (Fig. S4†). From the XRD patterns (Fig. 2g), both Pd/C and $Pd_{0.5}Cu_{0.5}$/C showed a broad peak located at around

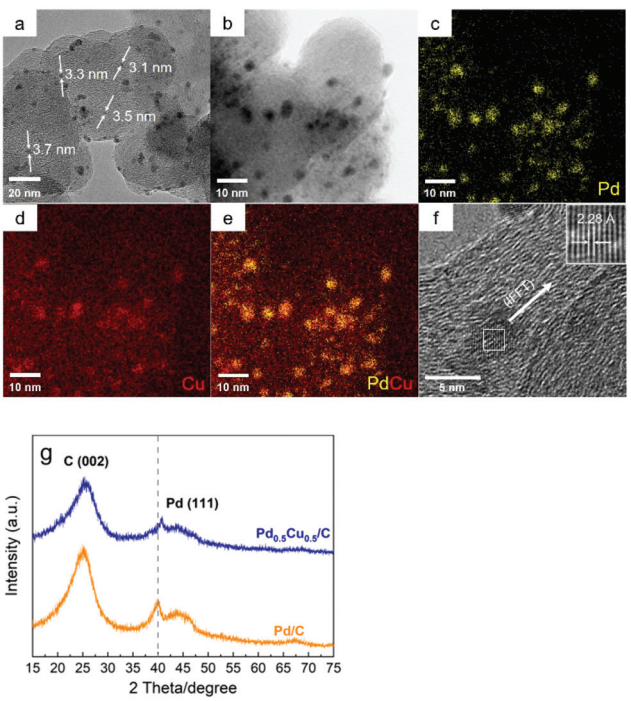

Fig. 2 TEM image (a), TEM-EDS elemental mapping (b–e), HRTEM image (f), and XRD patterns (g) of the as-synthesized $Pd_{0.5}Cu_{0.5}$/C catalyst.

This journal is © The Royal Society of Chemistry 2021

Published on 19 novembro 2020. Downloaded on 03/09/2024 17:48:12.

25°, which was attributed to the (002) plane of carbon with a hexagonal structure. The diffraction pattern of Pd/C showed a weak peak located at around 40°, which is attributed to the (111) plane of Pd's face-centred cubic (fcc) structure (ICDD 46-1043). On the other hand, Pd alloyed with Cu caused the diffraction peaks of Pd in the $Pd_{0.5}Cu_{0.5}$/C catalyst to shift slightly to higher 2θ values. The ICP-OES analysis of $Pd_{0.5}Cu_{0.5}$/C revealed that the weight percentage of Pd and Cu were 4.46% and 2.68%, respectively, which were close to the desired values (Pd 4.5 wt% and Cu 3.0 wt%). In brief, a carbon-supported PdCu alloy NP catalyst was successfully synthesized.

3.2 HCO_3^- reduction with methanol over $Pd_{0.5}Cu_{0.5}$/C catalyst

The possibility of HCO_3^- reduction with methanol as the reductant and $Pd_{0.5}Cu_{0.5}$/C as the catalyst was investigated. The results showed that formate was successfully produced after the reaction as predicted, and the total formate concentration was 121.9 mmol L^{-1}. For comparison, formic acid production from methanol alone was investigated in the absence of $NaHCO_3$ (Table 1). However, only a negligible trace amount of formic acid was produced when CH_3OH reacted alone. Furthermore, even after 1 mol L^{-1} NaOH was added to adjust the reaction pH, only 21.1 mol L^{-1} formate was produced without the addition of $NaHCO_3$, which was much lower than that (121.9 mmol L^{-1}) obtained with $NaHCO_3$. These results indicated the participation of $NaHCO_3$ in the formation of formate. It should be noted that formate and formic acid displayed a single peak in the HPLC analysis (Fig. S5†). Since both formic acid and formate were produced from the reaction of methanol with HCO_3^- (eqn (1)), ^{13}C-qNMR measurement was performed to distinguish and quantify the $NaHCO_3$-sourced formate and CH_3OH-sourced formic acid. In a labelling experiment using $NaH^{13}CO_3$ (Fig. S6†), a strong signal associated with $H^{13}COO^-$ was observed at 171.2 ppm. The concentration of the $NaH^{13}CO_3$-sourced formate was determined to be 67.3 mmol L^{-1} by adding 50 mmol L^{-1} $CH_3{}^{13}COOH$ as an internal standard. Based on the $NaHCO_3$-sourced formate concentration determined by qNMR and the total formate concentration determined by HPLC, the quantification of $NaHCO_3$-sourced formate and CH_3OH-sourced formic acid is summarized in Table 1. The results revealed that the concentrations of the $NaHCO_3$-sourced formate and CH_3OH-sourced formic acid were 67.3 and 54.6 mmol L^{-1}, respectively, which indicates that a dual formation of formate/formic acid from $NaHCO_3$ and CH_3OH was achieved. In addition, formaldehyde (HCHO) was also detected by GC-MS, suggesting that CH_3OH was stepwise oxidized into formaldehyde and formic acid. It is encouraging that the selectivity of formate was nearly 100% although a trace amount of HCHO was detected in liquid samples. GC-TCD analysis was further performed on the gaseous samples, and only H_2 was observed (Table 1). These results indicate that the coexistence of $NaHCO_3$ and CH_3OH is beneficial and necessary for the formation of formate.

Table 1 Product distribution of $NaHCO_3$ reduction with methanol[a]

	Liquid products (mmol L^{-1})			Gaseous products (mL)
	Formate			
	$NaHCO_3$ sourced	CH_3OH sourced	HCHO	H_2
With $NaHCO_3$	67.3	54.6	Trace	10.1 ml
w/o $NaHCO_3$	—	Trace	—	Trace
w/o $NaHCO_3$[b]	—	21.1	Trace	13.5 ml

[a] Reaction conditions: 0.1 mol L^{-1} CH_3OH, 1 mol L^{-1} $NaHCO_3$, 50% water filling, 50 mg $Pd_{0.5}Cu_{0.5}$/C, 180 °C, and 16 h. [b] 1 mol L^{-1} NaOH was added to simulate the alkalinity induced by $NaHCO_3$.

3.3 Reaction characteristics and catalyst stability

To enhance the production of formate from the $NaHCO_3$ reduction with methanol, the effects of different reaction parameters such as reaction temperature, time (Fig. S7†) and catalyst amount (Fig. S8†) were investigated. The temperature profile shows that only a trace amount of formate was formed at 150 °C. Increasing the temperature significantly promoted the formation of formate, especially when the temperature exceeded 160 °C. On the other hand, when the temperature reached 180 °C, the formate production efficiency increased continuously with the extension of time. However, the reaction tended to slow down when the reaction time exceeded 16 h. At 200 °C, a high efficiency of 75% from $NaHCO_3$ was obtained. The results of the effect of catalyst amount showed that increasing the catalyst amount obviously promoted the production of formate. However, when the catalyst amount reached 50 mg, further increase in the catalyst amount had no significant effect on the reaction efficiency. The stability of the $Pd_{0.5}Cu_{0.5}$/C catalyst was further examined. Although a slight decrease in the formate production efficiency was observed in the second cycle, further decline was not observed in the following five cycles (Fig. S9†). The $Pd_{0.5}Cu_{0.5}$/C catalyst after the reaction was collected and analysed by SEM, TEM and XRD (Fig. S10†). The results showed that the morphology and crystallinity of the $Pd_{0.5}Cu_{0.5}$/C catalyst had no obvious change after the reaction. However, the TEM analysis revealed that the PdCu alloy slightly aggregated after the reaction, and the NP size increased to *ca.* 4.5 nm, which probably caused the decrease in the formate production efficiency in the second cycle. The ICP analysis of the liquid sample after the reaction discovered no dissolved Pd or Cu species. These results indicated that the $Pd_{0.5}Cu_{0.5}$/C catalyst was relatively stable.

3.4 Catalytic property and mechanism

Based on the detected intermediates of HCHO and H_2 (Table 1), the overall process of the CH_3OH reaction with $NaHCO_3$ could be divided into two parts: hydrogen generation from methanol oxidation, which contains two steps (eqn (2) and (3)), and HCO_3^- hydrogenation to formate (eqn (4)).

$$CH_3OH \rightarrow HCHO + H_2 \quad (2)$$

Published on 19 novembro 2020. Downloaded on 03/09/2024 17:48:12.

$$HCHO + H_2O \rightarrow HCOOH + H_2 \quad (3)$$

$$H_2 + NaHCO_3 \rightarrow HCOONa + H_2O \quad (4)$$

Then, the catalytic property of $Pd_{0.5}Cu_{0.5}$/C for these two parts was studied separately to explore the catalytic mechanism. First, H_2 production from methanol oxidation was investigated in the presence and absence of the $Pd_{0.5}Cu_{0.5}$/C catalyst. For comparison, the results obtained from the Pd/C, Cu/C catalyst were also used. As summarized in Table 2, only a trace amount of H_2 was produced in the absence of any catalyst and in the presence of carbon black (Table 2, entries 1 and 2). On the other hand, H_2 generation was clearly promoted when Pd/C, $Pd_{0.5}Cu_{0.5}$/C and Cu/C were used, and the $Pd_{0.5}Cu_{0.5}$/C catalyst exhibited the best performance (Table 2, entries 3–5). The TON for hydrogen generation obtained on $Pd_{0.5}Cu_{0.5}$/C was 1.4 and 3.8 times higher than those obtained on Pd/C and Cu/C, respectively. These results indicate that $Pd_{0.5}Cu_{0.5}$/C could effectively promote methanol hydrothermal re-forming for hydrogen generation. Subsequently, $NaHCO_3$ hydrogenation with *ex situ* gaseous H_2 on the $Pd_{0.5}Cu_{0.5}$/C, Pd/C, and Cu/C was studied. The results showed that no formate was produced in the absence of any catalyst, and a significant increase in the production of formate appeared in the presence of the $Pd_{0.5}Cu_{0.5}$/C catalyst (Table S2†). The above results demonstrated that the $Pd_{0.5}Cu_{0.5}$/C catalyst played an irreplaceable part in both H_2 generation from methanol and $NaHCO_3$ hydrogenation.

In addition, the effect of different Pd/Cu ratios (molar ratio) on hydrogen generation and formate production was tested (Table 2, entries 4, and 6–9). $Pd_{0.5}Cu_{0.5}$/C exhibited the highest catalytic activities in formate production, indicating that a 1 : 1 Pd/Cu ratio was the optimum condition (Table 2, entry 4). Notably, it was less sensitive for formate production when the molar ratio of Pd was higher than 50% (Table 2, entries 6 and 7).

Table 2 Hydrogen generation and formate production efficiency obtained from different catalysts[a]

Entry	Catalyst	TON of hydrogen generation[b] (mol H_2 per mol PdCu)	Formate production efficiency[c] (%)
1	None	Trace	Trace
2	Carbon black	Trace	Trace
3	Pd/C	10.4	46.3
4	$Pd_{0.5}Cu_{0.5}$/C	14.3	67.6
5	Cu/C	3.8	15.2
6	$Pd_{0.75}Cu_{0.25}$/C	12.8	67.0
7	$Pd_{0.66}Cu_{0.33}$/C	13.1	67.5
8	$Pd_{0.33}Cu_{0.66}$/C	9.0	38.1
9	$Pd_{0.25}Cu_{0.75}$/C	7.6	22.2
10[d]	$Pd_{0.5}Cu_{0.5}$/C	Trace	Trace

[a] H_2 generation and formate production are two independent experiments. [b] Reaction conditions: 0.1 mol L^{-1} CH_3OH, 1 mol L^{-1} NaOH, 50% water filling, 50 mg catalysts, 180 °C, and 16 h. [c] Reaction conditions: 0.1 mol L^{-1} CH_3OH, 1 mol L^{-1} $NaHCO_3$, 50% water filling, 50 mg catalysts, 180 °C, and 16 h. [d] Methanol was used as a solvent instead of water, and the other conditions are the same as mentioned in footnotes "b" and "c".

On the other hand, increasing the proportion of Cu could improve the efficiency of H_2 generation; however, excessive Cu was unfavourable for formate production. Therefore, Pd is the core component in the PdCu alloy catalyst, and the introduction of Cu not only effectively reduced the cost of the precious metal but also improved hydrogen generation and further formate production.

The interaction between Pd and Cu should have an indispensable role in hydrogen generation and $NaHCO_3$ hydrogenation. To further verify the property of the PdCu alloy, XPS analysis was conducted. Fig. 3 illustrates the XPS results of $Pd_{0.5}Cu_{0.5}$/C and Pd/C before the reaction. Compared to Pd/C, the Pd 3d peaks of PdCu alloy shifted to a lower binding energy. For Pd/C, the Pd $3d_{5/2}$ and Pd $3d_{3/2}$ peaks centred at 335.9 and 341.3 eV, respectively, while for $Pd_{0.5}Cu_{0.5}$/C, the position of the Pd $3d_{5/2}$ and Pd $3d_{3/2}$ peaks shifted to 335.3 and 340.6 eV, respectively. This is probably attributed to the smaller electron negativity of Cu as compared to that of Pd, which leads to an electron injection from Cu to Pd.[36,37] The XPS result of Cu can be found in Fig. S11.† These results indicated that the incorporation of Cu could change the electronic structure of Pd, further leading to a downward shift of the Pd d-band centre.[38] The shift of the d-band centre resulted in a decrease in the binding energy of hydrogen on the Pd surface, which positively improved the catalytic performance of Pd for hydrogen generation.[39,40] On the other hand, when compared to the unalloyed state, the electronic structure of Pd modified by Cu doping caused the Pd d-band centre to be far away from its Fermi level.[38,41] The farther the d-band centre of the transition metals to their Fermi level, the lower the adsorption energy on the transition metal surface for the C1 products.[42,43] Thus, the formate adsorption enthalpy on the PdCu alloy surface became lower than that on pure Pd. As a result, when formate was formed on the PdCu alloy, it detached from the catalyst surface, leading to an enhanced formate production and selectivity of formate from HCO_3^- reduction. In brief,

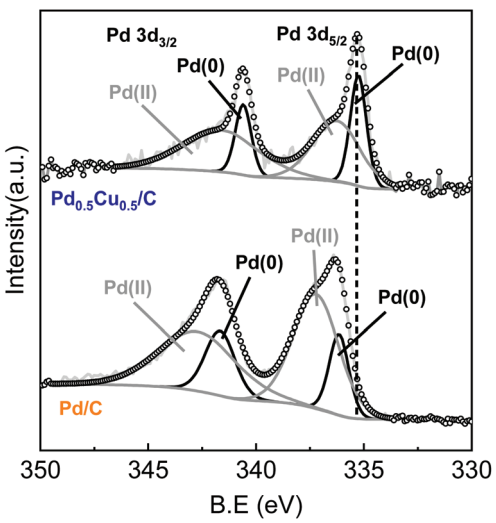

Fig. 3 XPS spectra of Pd 3d in $Pd_{0.5}Cu_{0.5}$/C and Pd/C.

This journal is © The Royal Society of Chemistry 2021

Published on 19 novembro 2020. Downloaded on 03/09/2024 17:48:12.

Pd should be the core reaction site for both the steps of hydrogen generation and formate production, while the introduction of Cu improved the Pd performance by altering the electronic structure of Pd.

3.5 Role of H_2O

As shown in eqn (3), one obvious role of H_2O was to react with HCHO to produce H_2, indicating that H_2O participated in the reaction as a hydrogen source. However, H_2 and HCHO were hardly detected when methanol reacted with HCO_3^- in the absence of H_2O (Table 2, entry 10), indicating that H_2O was also indispensable for the first step of methanol activation (eqn (2)). To further verify the role of H_2O and its mechanism, DFT calculations were performed on the process of hydrogen generation from methanol with or without H_2O. The structures of the methanol molecule, the transition state without H_2O, and the transition state with H_2O were determined, which are shown in Fig. 4a, b, and c, respectively. The transition state structure exhibited a narrow angle of 1C–5O–6H in the absence of H_2O (Fig. 4b), which was significantly bent (from 108.9° to 53.6°) as compared to that of the equilibrium structure of the isolated methanol (Fig. 4a). This result indicates that H_2 generation from methanol without H_2O requires overcoming a huge potential energy barrier. On the other hand, the 1C–5O–6H angle relaxed to 106.4° in the presence of H_2O (Fig. 4c), which is nearly comparable to that of the isolated methanol. Moreover, the added H_2O molecule (7O–8H–9H) behaves as a proton acceptor and formed a deformed H_3O-cation-like conformation with the transition state atom 6H from the methanol molecule, which would drastically reduce the activation energy for the ionic water dissociation. As a result of these effects, the energy barrier of hydrogen generation from methanol with H_2O addition was significantly reduced (from 378 kJ mol^{-1} to 220 kJ mol^{-1}) compared to that in the absence of H_2O (Fig. 4d), suggesting the critical role of H_2O as a promoter in this process. Then, the corresponding reaction mechanism based on the calculation results is proposed in Fig. 4d. One H_2O molecule acts as a bridge for methanol breaking down to produce one H_2 and one HCHO. Thus, it is suggested that the H_2 generated from methanol in eqn (2) should consist of one atom from methanol and one atom from H_2O. Based on these results, eqn (2)–(4) could be rewritten as isotope-labelled forms (eqn (5)–(7)) for a better understanding of the mechanism, in which D_2O and $NaH^{13}\underline{C}O_3$ were used instead of H_2O and $NaHCO_3$, respectively. This leads to the $NaH^{13}\underline{C}O_3$-sourced formate consisting of $H^{13}\underline{C}OO^-$ and $D^{13}\underline{C}OO^-$ in the ratio of 1 : 1.

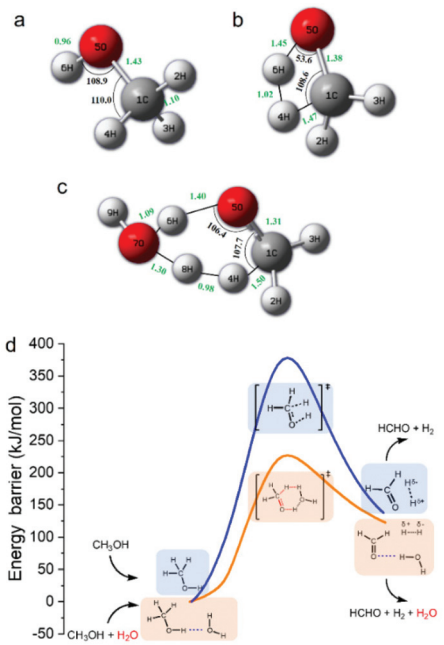

Fig. 4 Transition states (a)–(c) and energy profiles (d) for methanol dissociation into H_2 with or without H_2O (a: methanol molecule; b: the transition state without H_2O; c: the transition state with H_2O; and d: the profile with H_2O as the promoter is depicted in orange, while the profile without H_2O is depicted in blue).

$$CH_3OH + D_2O \rightarrow HCHO + DH + DHO \quad (5)$$

$$HCHO + D_2O \rightarrow HCOOD + DH \quad (6)$$

$$2DH + 2NaH^{13}\underline{C}O_3 \rightarrow H^{13}\underline{C}OONa + D^{13}\underline{C}OONa + DHO + H_2O \quad (7)$$

To further confirm the DFT calculation results and the above assumption (eqn (5)–(7)), isotopic tracing reaction with D_2O substituting H_2O was conducted. In the meantime, $NaH^{13}\underline{C}O_3$ was used instead of $NaHCO_3$ to trace the reaction path of carbon. It should be noted first that we confirmed that the H of $-CH_3$ in CH_3OH, –CH in HCHO or $HCOO^-$ would not undergo a hydrogen–deuterium exchange under hydrothermal conditions in an independent run (Fig. S12†). As displayed in Fig. 5a, the peak assigned to $D^{13}\underline{C}OO^-$ was clearly observed in the D-qNMR spectrum, and it consisted of two parallel peaks, while the corresponding ^{13}C-qNMR image showed that $NaH^{13}\underline{C}O_3$-sourced formate contained three parallel peaks, which was caused by the resonance effect between ^{13}C and D (Fig. 5a and b). The COSY spectra of the liquid sample after $NaH^{13}\underline{C}O_3$ had reacted with methanol in D_2O is also shown in Fig. 5c. These results confirmed that formate from $NaHCO_3$ reduction carried D from D_2O. Furthermore, the concentrations of D-labelled and ^{13}C-labelled formate were determined with dimethyl sulfoxide-D6 and $CH_3{}^{13}\underline{C}OOH$ as the internal standards, respectively.[44] The results showed that the final product of formate comprised of a nearly identical amount of $H^{13}\underline{C}OO^-$ and $D^{13}\underline{C}OO^-$ (Table 3), which was perfectly consistent with the DFT calculations and further confirmed the promoting effect of H_2O in methanol activation.

In summary, the results of DFT and ^{13}C/^{2}H-qNMR clearly demonstrated that H_2O served as a promoter for methanol activation in eqn (2). Thus, the total three roles of H_2O in the process of HCO_3^- reduction with methanol can be summarized as follows: (1) acting as an indispensable promoter by lowering the reaction energy barrier of methanol activation into

Published on 19 novembro 2020. Downloaded on 03/09/2024 17:48:12.

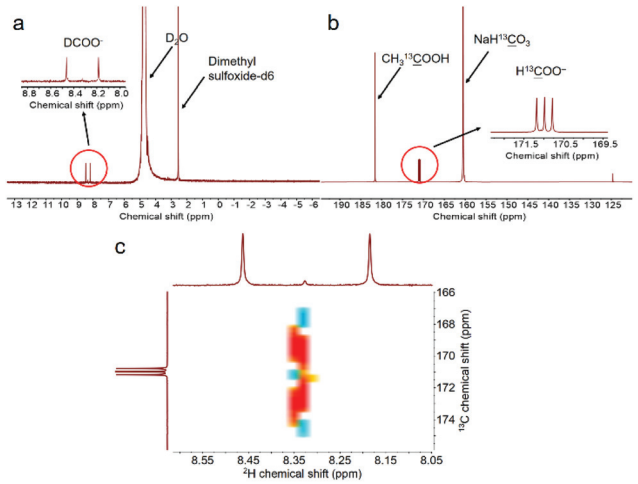

Fig. 5 D-qNMR (a), ^{13}C-qNMR (b) and COSY spectra (c) of the liquid sample after $NaH^{13}CO_3$ reaction with methanol in D_2O (reaction conditions: 0.1 mol L^{-1} CH_3OH, 1 mol L^{-1} $NaH^{13}CO_3$, 50% D_2O filling, 50 mg $Pd_{0.5}Cu_{0.5}$/C, 180 °C, and 16 h; dimethyl sulfoxide-D6 and $CH_3{}^{13}COOH$ were used as the internal standards to calculate the D-labelled and ^{13}C-labelled formate concentrations, respectively).

Table 3 Product distribution of $NaH^{13}CO_3$ reduction with methanol in D_2O[a]

Formate concentration (mmol L^{-1})	$NaH^{13}CO_3$ sourced		CH_3OH sourced	Total
	$H^{13}COO^-$	$D^{13}COOH^-$		
	33.3	32.1	53.1	118.5

[a] Reaction conditions: 0.1 mol L^{-1} CH_3OH, 1 mol L^{-1} $NaH^{13}CO_3$, 50% D_2O filling, 50 mg $Pd_{0.5}Cu_{0.5}$/C, 180 °C, and 16 h.

formaldehyde; (2) reacting with formaldehyde to release hydrogen; and (3) serving as a green solvent.

It should be noted that according to eqn (1), the ratio of CH_3OH-sourced HCOOH to HCO_3^--sourced $HCOO^-$ should be 1 : 2. However, our isotopic results showed that the actual ratio of CH_3OH-sourced HCOOH to HCO_3^--sourced $HCOO^-$ was *ca.* 1 : 1.2. These results suggested that in the reduction of HCO_3^- with CH_3OH, the first part (eqn (2) and (3)) was easier to react than the second part (eqn (4)). Thus, the unreacted H_2 product was detected in the gaseous phase.

3.6 *Operando* ATR-FTIR study

To obtain a full understanding of the reaction mechanism, an *operando* hydrothermal ATR-FTIR was further carried out to examine the transformation of the reactants. All the *operando* ATR-FTIR spectra were recorded as a subtraction spectrum with the initial state (25 °C, before starting the heating reaction) as the background. First, the spectra during the reaction with or without the catalyst were captured. As shown in Fig. 6a, the peaks at 1633 cm^{-1} and 1400 cm^{-1} are assigned to the asymmetrically and symmetrically adsorbed HCO_3^- (COO bond), respectively.[45,46] The 1012 cm^{-1} peak can be ascribed to

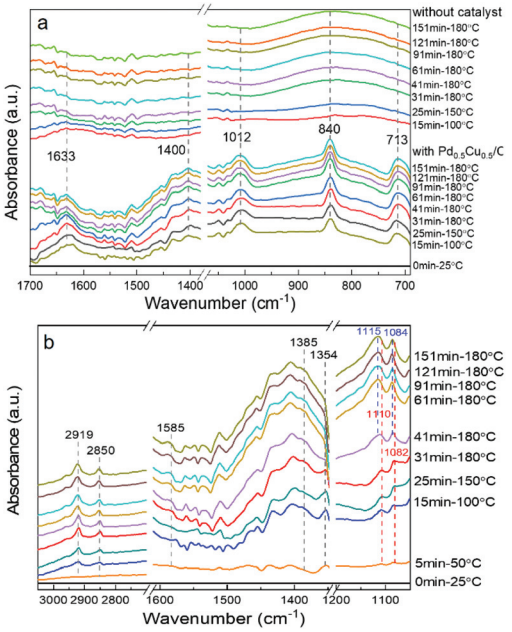

Fig. 6 *Operando* ATR-FTIR subtraction spectra recorded during HCO_3^- reduction with methanol (all the spectra subtracted the spectrum of the initial state as the background; initial state: 0.1 mol L^{-1} CH_3OH, 1 mol L^{-1} $NaHCO_3$, 100% water filling, 5 mg $Pd_{0.5}Cu_{0.5}$/C, 25 °C; (a) ATR-FTIR spectra comparison with or without the catalyst; (b) temperature and time sequence spectra of the *operando* ATR-FTIR obtained with the $Pd_{0.5}Cu_{0.5}$/C catalyst. Test conditions: 0.1 mol L^{-1} CH_3OH, 1 mol L^{-1} $NaHCO_3$, 100% water filling, 5 mg $Pd_{0.5}Cu_{0.5}$/C).

the C–O bond of the adsorbed CH_3OH, and the vibration signals caused by the metal–O bond at 840 cm^{-1} and 713 cm^{-1} also confirmed the adsorption of methanol on the catalyst surface.[47] Furthermore, the vibration peak due to the adsorption of reactants tended to weaken as the reaction proceeded, indicating that HCO_3^- and CH_3OH were consumed for further reaction on the $Pd_{0.5}Cu_{0.5}$/C surface.

Then, as shown in Fig. 6b, upon heating the mixture of CH_3OH and $NaHCO_3$ in aqueous solution, the peaks located at 1585 cm^{-1} and 1385 cm^{-1}, which represented the OCO asymmetric and symmetric stretches of $HCOO^-$, appeared and intensified gradually with increasing temperature, and the peak of the C–H bond stretching vibration at 2850 cm^{-1} related to $HCOO^-$ also increased gradually. These results indicate that formate production rate was promoted with increasing temperature and time. The main formaldehyde bands are located at 2923, 2853, and 1354 cm^{-1} based on the previous report;[48] however, the peaks at 2923 and 2853 cm^{-1} overlapped with the formate ν(C–H) bands in Fig. 6b, indicating that they were difficult to distinguish. On the other hand, the band at 1354 cm^{-1}, belonging to ω(C–H) of formaldehyde, was clearly observed at 100 °C and its absorbance signal increased with the reaction temperature. Nevertheless, when temperature reached 180 °C, the formaldehyde vibration disappeared with prolonged time; this was probably attributed to the rapid transformation of formaldehyde to formate during the reac-

 This journal is © The Royal Society of Chemistry 2021

Published on 19 novembro 2020. Downloaded on 03/09/2024 17:48:12.

tion, making it difficult to capture. Furthermore, the peaks at 1110 and 1082 cm^{-1}, which could be assigned to the C–O bond of methanol, was blue-shifted along with the increase in reaction time. This was probably attributed to the methanol oxidation into formaldehyde, that is, the transformation from the C–O bond to the C═O bond, causing the increase in the bonding energy of the C–O bond.

3.7 Reaction mechanism

Based on the above research, a possible reaction mechanism of the HCO_3^- reaction with methanol in water on $Pd_{0.5}Cu_{0.5}/C$ is proposed in Fig. 7. First, CH_3OH (i) is oxidized into HCHO (iii) on the catalyst with H_2 generation through the promotion effect of a H_2O molecule. Then, the formed HCHO (iii) reacts with a second H_2O molecule to produce another H_2 and HCOOH (v). Thus, one CH_3OH molecule produces two molecules of H_2 with one H_2O molecule as the promoter and another as the hydrogen source. Subsequently, the formed *in situ* H_2 and HCO_3^- are activated by adsorbing on the $Pd_{0.5}Cu_{0.5}/C$ surface ((vii) and (viii)), and then the activated H nucleophilic attacks the C═O, leading to the formation of $HCOO^-$ ((ix) and (x)) through the cleavage of the C–OH bond.

3.8 Universality research

The applicability of hydrothermal reduction of various inorganic carbon sources with different alcohols was examined. As summarized in Table 4, when gaseous CO_2 was used as the starting material instead of bicarbonate, only a trace amount of formate was detected (Table 4, entry 2), suggesting it was difficult for CO_2 gas to be directly converted in this system. However, when 1 mol L^{-1} NaOH was added, 48.6% formate production efficiency was successfully obtained (Table 4, entry 3), which should be attributed to the transformation of CO_2 to HCO_3^- in NaOH solution. This result further suggests that a one-step CO_2 capture and conversion reaction can be achieved by using the presented method. Furthermore, other carbonates and bicarbonates such as K_2CO_3, $KHCO_3$, and Na_2CO_3 were also tested, and the formate production efficiency reached 87.3%, 70.5% and 83.4%, respectively (Table 4, entries 4–6). Notably, the hydrogenation of carbonates is generally more difficult than that of bicarbonates because the protonation of carbonate ions was considered to be inferior in aqueous solutions.[49,50] To our delight, the carbonates showed better performance than the corresponding bicarbonates in the presented research. This is probably because the weak acidity of methanol was enhanced by the hydrothermal reaction, which then attacked the inert CO_3^{2-} and made it more reactive than the *ex situ* HCO_3^-.

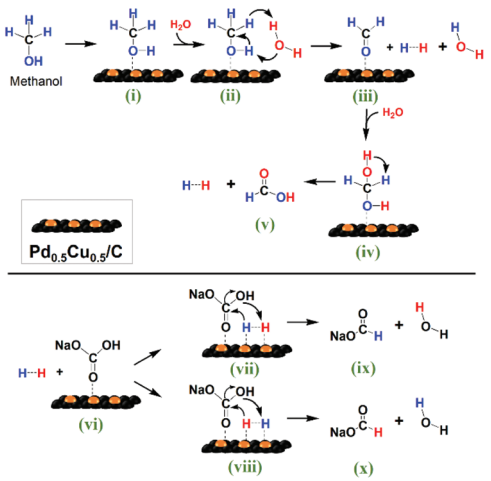

Fig. 7 Reaction scheme of HCO_3^- reduction into formate with methanol in water on the $Pd_{0.5}Cu_{0.5}/C$ catalyst.

Table 4 Reduction of various CO_2 sources with different alcohols[a]

Entry	Alcohols	Carbon source[b]	Formate production efficiency (%)
1	Methanol	—	Trace
2	Methanol	CO_2	Trace
3[c]	Methanol	CO_2	48.6
4	Methanol	K_2CO_3	87.3
5	Methanol	$KHCO_3$	70.5
6	Methanol	Na_2CO_3	83.4
7	Methanol	$NaHCO_3$	67.6
8	Ethanol	$NaHCO_3$	68.9
9	1-Propanol	$NaHCO_3$	72.3
10	1-Butanol	$NaHCO_3$	73.4

[a] Reaction conditions: 0.1 mol L^{-1} alcohol, 1 mol L^{-1} HCO_3^- or CO_3^{2-}, 50% water filling, 50 mg $Pd_{0.5}Cu_{0.5}/C$, 180 °C, and 16 h. [b] CO_2: 2.5 MPa, others: 1 mol L^{-1}. [c] 1 mol L^{-1} NaOH was added.

In addition, the activity of various alcohols used as a reductant for the hydrothermal reduction of HCO_3^- was examined. The results revealed that ethanol, 1-propanol and 1-butanol exhibited similar activity to that of methanol in the reduction of HCO_3^- to formate, while were themselves converted to their corresponding acids (Table 4, entries 8–10, Fig. S13†). Notably, the reactivity of alcohols slightly increased with the growth of the carbon chains and 1-butanol exhibited the best activity for HCO_3^- reduction. Based on the above results, the alcohol-bicarbonate system can be expected to be applied to the synergistic conversion of various hydroxyl-rich organics and CO_2 sources.

4. Conclusions

In summary, we have developed an efficient strategy for HCO_3^- reduction with methanol as the hydrogen source on a $Pd_{0.5}Cu_{0.5}/C$ catalyst under mild hydrothermal conditions. A 68% formate production efficiency and nearly 100% selectivity of formate from bicarbonate were obtained *via* a $Pd_{0.5}Cu_{0.5}/C$ catalyst at 180 °C. Notably, the DFT calculations and qNMR studies confirmed that molecular H_2O not only supplied hydrogen but also acted as an indispensable promoter to enhance the catalytic performance of $Pd_{0.5}Cu_{0.5}/C$ for methanol activation. Furthermore, the *operando* ATR-FTIR revealed that the mechanism of methanol oxidation to generate hydro-

Published on 19 novembro 2020. Downloaded on 03/09/2024 17:48:12.

gen is $CH_3OH \rightarrow HCHO \rightarrow HCOOH$, and HCO_3^- is reduced into formate with the *in situ* formed hydrogen. The present study provided a potential way towards simple and green one-step CO_2 capture and utilization, which is of great interest in the practical application of CO_2 conversion.

Conflicts of interest

There are no conflicts to declare.

Acknowledgements

The authors thank the financial support of the National Key R&D Program of China (2018YFC0309800 and 2017YFC0506004), the National Natural Science Foundation of China (No. 21978170), the Natural Science Foundation of Shanghai (No. 19ZR1424800), the National Postdoctoral Program for Innovative Talent (No. BX20200208), the Oceanic Interdisciplinary Program of Shanghai Jiao Tong University (No. SL2020MS022), the Start-up Fund for Youngman Research at SJTU, and the Centre of Hydrogen Science, Shanghai Jiao Tong University, China.

Notes and references

1 A. Barthel, Y. Saih, M. Gimenez, J. D. A. Pelletier, F. E. Kühn, V. D'Elia and J. M. Basset, *Green Chem.*, 2016, **18**, 3116–3123.
2 D. W. Keith, G. Holmes, D. S. Angelo and K. Heidel, *Joule*, 2018, **2**, 1573–1594.
3 E. S. Sanz-Perez, C. R. Murdock, S. A. Didas and C. W. Jones, *Chem. Rev.*, 2016, **116**, 11840–11876.
4 S. Das, J. Pérez-Ramírez, J. Gong, N. Dewangan, K. Hidajat, B. C. Gates and S. Kawi, *Chem. Soc. Rev.*, 2020, **49**, 2937–3004.
5 M. Ding, R. W. Flaig, H.-L. Jiang and O. M. Yaghi, *Chem. Soc. Rev.*, 2019, **48**, 2783–2828.
6 H. Zhong, K. Fujii and Y. Nakano, *J. Electrochem. Soc.*, 2017, **164**, F923–F927.
7 S. H. Kim, K. H. Kim and S. H. Hong, *Angew. Chem., Int. Ed.*, 2014, **53**, 771–774.
8 H. Zhong, K. Fujii, Y. Nakano and F. Jin, *J. Phys. Chem. C*, 2015, **119**, 55–61.
9 H. Zhong, M. Iguchi, M. Chatterjee, Y. Himeda, Q. Xu and H. Kawanami, *Adv. Sustainable Syst.*, 2018, **2**, 1700161.
10 H. Zhong, M. Iguchi, M. Chatterjee, T. Ishizaka, M. Kitta, Q. Xu and H. Kawanami, *ACS Catal.*, 2018, **8**, 5355–5362.
11 R. Navarro, M. Sanchez-Sanchez, M. Alvarez-Galvan, F. Del Valle and J. Fierro, *Energy Environ. Sci.*, 2009, **2**, 35–54.
12 S. Choi, T. C. Davenport and S. M. Haile, *Energy Environ. Sci.*, 2019, **12**, 206–215.
13 G. W. Huber, J. Shabaker and J. Dumesic, *Science*, 2003, **300**, 2075–2077.
14 D. M. Alonso, J. Q. Bond and J. A. Dumesic, *Green Chem.*, 2010, **12**, 1493–1513.
15 F. Jin, Y. Gao, Y. Jin, Y. Zhang, J. Cao, Z. Wei and R. L. Smith Jr., *Energy Environ. Sci.*, 2011, **4**, 881.
16 J. Duo, F. Jin, Y. Wang, H. Zhong, L. Lyu, G. Yao and Z. Huo, *Chem. Commun.*, 2016, **52**, 3316–3319.
17 H. Zhong, L. Wang, Y. Yang, R. He, Z. Jing and F. Jin, *ACS Appl. Mater. Interfaces*, 2019, **11**, 42149–42155.
18 H. Zhong, G. Yao, X. Cui, P. Yan, X. Wang and F. Jin, *Chem. Eng. J.*, 2019, **357**, 421–427.
19 M. Wang, M. Liu, J. Lu and F. Wang, *Nat. Commun.*, 2020, **11**, 1–9.
20 M. Liu, Y. Wang, X. Kong, R. T. Rashid, S. Chu, C.-C. Li, Z. Hearne, H. Guo, Z. Mi and C. J. Li, *Chem*, 2019, **5**, 858–867.
21 Z. Luo, Y. Ouyang, H. Zhang, M. Xiao, J. Ge, Z. Jiang, J. Wang, D. Tang, X. Cao and C. Liu, *Nat. Commun.*, 2018, **9**, 1–8.
22 N. J. Johnson, B. Lam, B. P. MacLeod, R. S. Sherbo, M. Moreno-Gonzalez, D. K. Fork and C. P. Berlinguette, *Nat. Mater.*, 2019, **18**, 454–458.
23 J. D. A. Pelletier and J. Basset, *Acc. Chem. Res.*, 2016, **49**, 664–677.
24 M. K. Samantaray, V. Delia, E. Pump, L. Falivene, M. Harb, S. O. Chikh, L. Cavallo and J. Basset, *Chem. Rev.*, 2020, **120**, 734–813.
25 S. Kattel, P. Liu and J. G. Chen, *J. Am. Chem. Soc.*, 2017, **139**, 9739–9754.
26 T. Schedel-Niedrig, M. Hävecker, A. Knop-Gericke and R. Schlögl, *Phys. Chem. Chem. Phys.*, 2000, **2**, 3473–3481.
27 H. Bluhm, M. Hävecker, A. Knop-Gericke, E. Kleimenov, R. Schlögl, D. Teschner, V. I. Bukhtiyarov, D. F. Ogletree and M. Salmeron, *J. Phys. Chem. B*, 2004, **108**, 14340–14347.
28 H. Duan, J. C. Liu, M. Xu, Y. Zhao, X. L. Ma, J. Dong, X. Zheng, J. Zheng, C. S. Allen, M. Danaie, Y. K. Peng, T. Issariyakul, D. Chen, A. I. Kirkland, J. C. Buffet, J. Li, S. C. E. Tsang and D. O'Hare, *Nat. Catal.*, 2019, **2**, 1078–1087.
29 F. Jin and H. Enomoto, *Energy Environ. Sci.*, 2011, **4**, 382–397.
30 Y. Zhang, Z. Shen, X. Zhou, M. Zhang and F. Jin, *Green Chem.*, 2012, **14**, 3285–3288.
31 L. Lu, H. Zhong, T. Wang, J. Wu, F. Jin and T. Yoshioka, *Green Chem.*, 2020, **22**, 352–358.
32 F. M. Jin, A. Kishita, T. Moriya and H. Enomoto, *J. Supercrit. Fluids*, 2001, **19**, 251–262.
33 N. Yang, Z. Zhang, B. Chen, Y. Huang, J. Chen, Z. Lai, Y. Chen, M. Sindoro, A. L. Wang and H. Cheng, *Adv. Mater.*, 2017, **29**, 1700769.
34 X. Huang, S. Tang, X. Mu, Y. Dai, G. Chen, Z. Zhou, F. Ruan, Z. Yang and N. Zheng, *Nat. Nanotechnol.*, 2011, **6**, 28.
35 W.-C. Cheong, C. Liu, M. Jiang, H. Duan, D. Wang, C. Chen and Y. Li, *Nano Res.*, 2016, **9**, 2244–2250.
36 Z. Guo, X. Kang, X. Zheng, J. Huang and S. Chen, *J. Catal.*, 2019, **374**, 101–109.
37 F. Pang, Z. Wang, K. Zhang, J. He, W. Zhang, C. Guo and Y. Ding, *Nano Energy*, 2019, **58**, 834–841.

 This journal is © The Royal Society of Chemistry 2021

38 J. Fan, S. Yu, K. Qi, C. Liu, L. Zhang, H. Zhang, X. Cui and W. Zheng, *J. Mater. Chem. A*, 2018, **6**, 8531–8536.
39 G. W. Huber, J. W. Shabaker, S. T. Evans and J. A. Dumesic, *Appl. Catal., B*, 2006, **62**, 226–235.
40 J. Greeley and M. Mavrikakis, *Nat. Mater.*, 2004, **3**, 810–815.
41 X. Yu, X. Tian and S. Wang, *Surf. Sci.*, 2014, **628**, 141–147.
42 G. C. Wang, Y. H. Zhou and J. Nakamura, *J. Chem. Phys.*, 2005, **122**, 044707.
43 H. Ma, G. Wang, Y. Morikawa and J. Nakamura, *Sci. China, Ser. B: Chem.*, 2009, **52**, 1427–1433.
44 Y. Yang, H. Zhong, R. He, X. Wang, J. Cheng, G. Yao and F. Jin, *Green Chem.*, 2019, **21**, 1247–1252.
45 A. Rodes, E. Pastor and T. Iwasita, *J. Electroanal. Chem.*, 1994, **376**, 109–118.
46 L. F. Liao, C. F. Lien, D. L. Shieh, M. T. Chen and J. L. Lin, *J. Phys. Chem. B*, 2002, **106**, 11240–11245.
47 N. A. Anan, S. M. Hassan, E. M. Saad, I. S. Butler and S. I. Mostafa, *Carbohydr. Res.*, 2011, **346**, 775–793.
48 J. De Souza, S. Queiroz, K. Bergamaski, E. R. Gonzalez and F. C. Nart, *J. Phys. Chem. B*, 2002, **106**, 9825–9830.
49 T. Wang, D. Ren, Z. Huo, Z. Song, F. Jin, M. Chen and L. Chen, *Green Chem.*, 2017, **19**, 716–721.
50 J. Su, M. Lu and H. Lin, *Green Chem.*, 2015, **17**, 2769–2773.

Published on 19 novembro 2020. Downloaded on 03/09/2024 17:48:12.